

# Twenty Years of Trials and Insights: Bridging Legacy and Next Generation in ParFlow and Land Surface Model Coupling

Chen Yang<sup>1\*</sup>, Aoqi Sun<sup>1</sup>, Shupeng Zhang<sup>1</sup>,  
Yongjiu Dai<sup>1</sup>, Stefan Kollet<sup>2,3</sup>, Reed Maxwell<sup>4</sup>

<sup>1</sup>School of Atmospheric Sciences, Sun Yat-sen University, Zhuhai, China

<sup>2</sup>Institute of Bio- and Geosciences (IBG-3, Agrosphere), Forschungszentrum Jülich (FZJ), Jülich, Germany

<sup>3</sup>Center for High-Performance Scientific Computing in Terrestrial Systems (HPSC TerrSys), Geoverbund ABC/J, Jülich, Germany

<sup>4</sup>Department of Civil and Environmental Engineering, The High Meadows Environmental Institute and the Integrated GroundWater Modeling Center, Princeton University, Princeton, USA

\*Corresponding to: yangch329@mail.sysu.edu.cn

## Abstract

Groundwater plays a vital role in terrestrial water and energy cycles. Yet, it remains oversimplified in most Earth system models (ESMs), limiting their ability to represent key land-atmosphere interactions, including evapotranspiration partitioning, drought propagation, and boundary layer development. The original coupling of ParFlow with the Common Land Model (CoLM) in 2005 not only demonstrated the feasibility of integrating physically based groundwater models into ESMs, but also revealed emergent behaviors—such as lateral moisture redistribution, along with the buffering effects that emerge from enhanced subsurface connectivity—that cannot be captured by traditional land surface models (LSMs). This study reviews key findings from two decades of ParFlow–land/atmosphere coupled modeling efforts, highlighting how groundwater–land–atmosphere interactions shape surface energy balance and hydrologic connectivity across three dimensions: upward feedbacks, downward influences, and the critical zone of coupling. Given the substantial advances in LSMs such as CoLM over the past two decades, a renewed recoupling effort is warranted to enhance our understanding of groundwater’s role across a broader range of Earth system processes. Preliminary efforts to recouple ParFlow with the updated water and energy modules of CoLM demonstrate improved performance when evaluated against reanalysis and observational data. To ensure long-term sustainability, we propose a modular and maintainable coupling framework addressing functional extensibility, data/code interoperability, and parallel computing needs, in which area, TerrSysMP2 has taken early steps and may be considered an initial forerunner. Finally, we summarize existing ParFlow-based coupled systems and highlight the need for a community-led model intercomparison project (PLCMIP) to benchmark performance, evaluate process coupling under varied configurations, and foster cross-community collaboration.

Deleted: ,

Deleted: y

44 **1. Introduction**

45 In 2005, Maxwell and Miller published "Development of a Coupled Land Surface and  
46 Groundwater Model" in *Journal of Hydrometeorology* (Maxwell and Miller, 2005). Their work  
47 introduced the first coupling of ParFlow (Ashby and Falgout, 1996; Jones and Woodward, 2001)  
48 and the Common Land Model (CLM) (Dai et al., 2003), and validated the framework using both  
49 synthetic and real-world test cases. The study highlighted the importance of groundwater  
50 representation in land surface processes (Fan et al., 2019; Zeng et al., 2018; De Graaf and  
51 Stahl, 2022; Seuffert et al., 2002). In particular, it emphasized the role of lateral subsurface flow  
52 (Figure 1), a component that was not explicitly represented in most land surface models (LSMs)  
53 at the time. This work represented an early step toward incorporating physically based  
54 groundwater dynamics into Earth system modeling frameworks.

55 Since LSMs serve as the lower boundary in ESMs, this coupling provided a practical  
56 pathway to incorporate groundwater dynamics into larger-scale Earth system frameworks.  
57 Compared to earlier coupling attempts based on tightly integrated or proprietary platforms (Yeh  
58 and Eltahir, 2005; Ivanov et al., 2004; York et al., 2002), this effort leveraged established  
59 community models and an open design philosophy, facilitating broader applicability and long-  
60 term adaptability. The resulting ParFlow-CLM model and other subsequent models coupled  
61 with ParFlow have been applied in a range of hydrological and land-atmosphere studies  
62 (Maxwell et al., 2007; Maxwell et al., 2011; Shrestha et al., 2014), contributing to improved  
63 understanding of water and energy exchanges across subsurface, land surface, and  
64 atmospheric domains (Rahman et al., 2015; Sulis et al., 2017; Keune et al., 2016; Forrester  
65 and Maxwell, 2020). Even today, groundwater-land surface coupling remains underutilized in  
66 many large-scale modeling frameworks, where groundwater models are often run offline with  
67 limited interaction with land-atmosphere processes (De Graaf et al., 2017; Reinecke et al.,  
68 2019; Verkaik et al., 2022), thereby missing dynamic feedbacks with the land-atmosphere  
69 system.

70 The groundwater model, ParFlow, simulates fully 3D variably saturated subsurface flow  
71 and overland flow by integrating Richards' equation with the shallow water equation in a unified  
72 numerical framework (Kollet and Maxwell, 2006; Osei-Kuffuor et al., 2014; Maxwell, 2013).  
73 Meanwhile, the Common Land Model (CLM, now CoLM) captures water and energy processes  
74 from the canopy top to the bottom of the root zone. These two models were coupled through  
75 the root zone (Figure 1), where net fluxes from CoLM after the interactions of infiltration and  
76 evapotranspiration (ET) are treated as source/sink terms in ParFlow, while ParFlow returns soil  
77 moisture and pressure head to CoLM to close the water and energy balance. Such a coupling  
78 approach in terms of physics has been widely adopted by the following coupling works (Niu et  
79 al., 2014; Fang et al., 2022; Maina et al., 2025).

80 After two decades of continuous development, LSMs such as CoLM have seen substantial  
81 advancements in functionality, code architecture, data structures, I/O systems, pre-/post-  
82 processing tools, and high-performance computing capabilities. ParFlow has undergone similar

Deleted: ¶

Deleted: a study titled

Deleted: was published

Deleted: It

Deleted: role

Deleted: ,

Deleted: ly

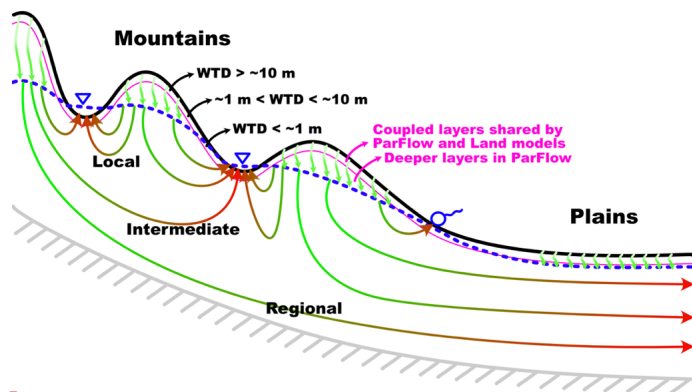
Deleted: —

Deleted: .

92 progress on the hydrological modeling front (Kuffour et al., 2020). Although the original coupling  
93 between ParFlow and CoLM was once considered sustainable, it is now increasingly  
94 inadequate as both models continue to grow in complexity and scope.

95 At this twenty-year juncture, it is necessary to re-examine the current state of the coupled  
96 system and clarify how the next stage of development should proceed. This involves, first,  
97 synthesizing the scientific findings enabled by the coupled framework over the past two  
98 decades to fully understand its importance for groundwater–land–atmosphere interactions. It  
99 also requires an initial assessment of the new coupling—particularly its physical functionality  
100 and performance—to clarify the benefits of moving forward. Finally, it is essential to consider  
101 how future recoupling can be made sustainable. Together, these steps will support a cross-  
102 disciplinary effort that provides a robust platform for the broader community to apply coupled  
103 models efficiently, pursue advanced Earth system questions, and strengthen collaborative  
104 research. Here we take CoLM as an example to present this transitional effort.

Deleted: in the face of growing model complexity and volume. In light of these developments, we outline a sustainable framework to support the next stage of ParFlow-LSM coupling development, with CoLM serving as a primary example. This cross-disciplinary effort is expected to provide a robust platform for the broader scientific community to efficiently apply coupled models, pursue advanced Earth system inquiries, and strengthen collaborative research. Given the scope of this task, implementation will necessarily proceed in phases.



Deleted: ¶

105 **Figure 1.** Illustration of the lateral groundwater flow, the critical zone of water table depth,  
106 and the coupling strategy between ParFlow and land surface models. Modified from  
107 Yang et al. (2023).  
108

109 In this paper, we begin by reviewing key insights gained from two decades of research  
110 involving ParFlow-based coupled modeling systems. Building on this foundation, we highlight  
111 how increasing model complexity and functionality are driving a shift toward a next-generation  
112 coupling paradigm. We then present a re-coupling of the latest versions of ParFlow (PF) and  
113 CoLM, focusing on core functionalities of CoLM to demonstrate feasibility and highlight  
114 improvements in overall model performance. This science-oriented integration of basic  
115 modules—built upon the original coupling interface—serves as a foundation for broader re-  
116 coupling efforts that will incorporate additional functional components under a redesigned,  
117 sustainable coupling framework. It also helps us better understand how both models have  
118 evolved since their original coupling in 2005, thereby informing the development of a next-  
119 generation framework. In recognition of the increasing number of LSMs being coupled with  
120 ParFlow, we further propose a ParFlow-Land Surface Coupled Model Intercomparison Project  
121 (PLCMIP) to promote collaboration and knowledge exchange across the community.

134 **2. A brief review of ParFlow-Land/Atmosphere coupled modeling**

135 The coupled model provides a more realistic representation of groundwater dynamics than  
136 traditional LSMs, while also offering more advanced ecohydrological processes at the land  
137 surface than conventional groundwater models. Over the past two decades, its major scientific  
138 contributions can be summarized in three key areas:

139 (1) It captures the feedbacks from groundwater to land and atmospheric processes—an  
140 area often overlooked or omitted in both atmospheric and groundwater research  
141 communities.

142 (2) It highlights the critical range of water table depth (WTD) that mediates these feedbacks.

143 (3) It elucidates the impacts of land cover and climate change on groundwater and other  
144 complex ecohydrological interactions.

145 ~~Because this manuscript is designed to synthesize the past, present, and future of the~~  
146 ~~ParFlow-based coupled systems at this twenty-year juncture, this review primarily synthesizes~~  
147 ~~advances within the ParFlow-LSM and ParFlow-atmosphere modeling family, while also briefly~~  
148 ~~situating other groundwater-land coupling efforts in a broader community context.~~

149 **2.1 Feedbacks from groundwater to land surface and atmosphere**

150 ~~Adding groundwater representation in ESMs reshapes the spatiotemporal distribution of~~  
151 ~~soil moisture, which in turn controls surface turbulent fluxes and the evolution of the~~  
152 ~~atmospheric boundary layer (Forrester and Maxwell, 2020; Rihani et al., 2015). This is primarily~~  
153 ~~due to the limited simulation depth in LSMs and the absence of lateral groundwater flow. The~~  
154 ~~former limits drainage in ridge areas, resulting in insufficient water release and an~~  
155 ~~overestimation of soil moisture; the latter suppresses groundwater convergence in valley areas,~~  
156 ~~leading to underestimation of soil moisture there.~~

157 Generally, lateral groundwater flow enhances soil moisture in topographic lows,  
158 suppresses boundary layer development, and increases the evaporative fraction, thereby  
159 weakening land-atmosphere coupling and reducing near-surface temperatures (Forrester and  
160 Maxwell, 2020; Keune et al., 2016). These responses are further modulated by the subsurface  
161 hydraulic conductivities ( $K$ ), with more pronounced sensitivities to  $K$  under simplified  
162 groundwater parameterizations (Williams and Maxwell, 2011; Keune et al., 2016; Rihani et al.,  
163 2010). Notably, the impact of groundwater and subsurface properties on surface flux  
164 partitioning and boundary layer development tends to be most pronounced in the afternoon,  
165 when radiative forcing peaks and land-atmosphere interactions intensify (Rahman et al., 2015;  
166 Rihani et al., 2015; Forrester and Maxwell, 2020; Maxwell et al., 2007).

167 Forrester and Maxwell (2020) conducted WRF-based weather simulations over the  
168 mountainous regions of Colorado to investigate the impact of different lower boundary  
169 conditions, providing a detailed explanation of the processes mentioned above. The study

Formatted: Font: (Default) Arial Regular, (Asian) Arial Unicode MS, 10 pt, Not Bold

Formatted: Indent: First line: 0.25", No bullets or numbering

Formatted: Font: (Default) Arial Regular, (Asian) Arial Unicode MS, 10 pt, Not Italic, Font color: Auto

Formatted: Font: (Default) Arial Regular, (Asian) Arial Unicode MS, 10 pt, Not Italic, Font color: Auto

Formatted: Font: (Default) Arial Regular, (Asian) Arial Unicode MS, 10 pt, Not Italic, Font color: Auto

Formatted: Font: (Default) Arial Regular, (Asian) Arial Unicode MS, 10 pt, Not Italic, Font color: Auto

Formatted: Font: (Default) Arial Regular, (Asian) Arial Unicode MS, 10 pt, Not Italic, Font color: Auto

Formatted: Font: (Default) Arial Regular

Deleted: A major consensus in the community is that the representation of  $g$

Deleted: significantly affect

Deleted: thereby influencing

Deleted: such as latent and sensible heat, as well as

Deleted: spatiotemporal dynamics

176 included a baseline scenario and several comparative scenarios, with particular emphasis on  
177 one that used PF-WRF to explicitly represent three-dimensional groundwater flow. In the  
178 baseline scenario, conventional WRF simulation was employed, with the subsurface depth of  
179 2 m, divided into four layers with thicknesses of 0.1, 0.3, 0.6, and 1 m from top to bottom. The  
180 bottom boundary used the native Noah model setting, which allows free drainage and further  
181 adjusts fluxes based on terrain. In the PF-WRF scenario, the subsurface depth was increased  
182 to 102 meters by adding a fifth layer of 100 m in thickness, with the bottom boundary set as  
183 impermeable. The Noah model and ParFlow were coupled through the top four layers, resulting  
184 in a coupling depth of 2 m.

185 Simulation results showed that, in the PF-WRF scenario, enhanced drainage over ridge  
186 areas reduced soil moisture, while lateral groundwater convergence increased soil moisture in  
187 valleys. Correspondingly, the boundary layer height also exhibited increases in ridge areas and  
188 decreases in valley areas. These changes in soil moisture and boundary layer height showed  
189 significant seasonal variations. Furthermore, the results revealed that microtopography induced,  
190 highly heterogeneous local variations in soil moisture. This in turn, weakened the clear  
191 elevation-dependent trend observed in the baseline scenario.

192 Additionally, in the baseline scenario, the coupling strength between evaporative fraction  
193 (EF, the ratio of latent heat to the sum of latent and sensible heat) and boundary layer height  
194 was weakened or even reversed in the PF-WRF scenario. That is, the significant negative  
195 correlation between EF and boundary layer height decreased or turned positive; this may be  
196 due to the temporal variations in EF caused by lateral flow. Moreover, the PF-WRF scenario  
197 with lateral flow showed stronger morning mountain breezes (upslope) and valley breezes  
198 (downslope), which may have enhanced mountain-valley circulation. Lateral groundwater flow  
199 also modulated low-level convection in river valleys, particularly increasing convective available  
200 potential energy (CAPE) in the afternoon, thereby perturbing regional precipitation.

201 Keune et al. (2016) conducted simulations over the European CORDEX region using the  
202 TerrSysMP modeling system (Shrestha et al., 2014), setting up two scenarios: one with fully  
203 three-dimensional groundwater flow (3D) and the other with one-dimensional free drainage  
204 (FD). Similarly, their results revealed that different representations of groundwater led to  
205 variations in CAPE, indicating influences on the evolution of atmospheric boundary layer and  
206 free troposphere. The 3D scenario weakened land-atmosphere coupling, thereby suppressing  
207 the occurrence of extreme weather events, which is consistent with the findings of Forrester  
208 and Maxwell (2020). More specifically, the simulated 2 m air temperature was generally lower  
209 in the 3D scenario than in the FD scenario, providing useful insights for simulating European  
210 heatwaves during the study period.

211 The study also showed that model differences were primarily located in areas with shallow  
212 water tables (depth < 5 m), which aligns with findings of Forrester and Maxwell (2020) that  
213 humidity, potential temperature, and vertical wind exhibit more pronounced differences in  
214 mountainous valley regions. In addition, the study revealed that variations in deep soil (depth >

- Deleted: the
- Deleted: in
- Deleted: and
- Deleted: led to a de
- Deleted: in
- Deleted: over ridges and an increase over
- Deleted: under the influence of
- Deleted: ,
- Deleted: the
- Deleted: of
- Deleted: was highly heterogeneous,
- Deleted: ing
- Deleted: general
- Deleted: of soil moisture varying with elevation as see
- Deleted: n

230 3 m) hydraulic conductivities led to discrepancies in simulation results. The FD scenario was  
231 more sensitive to the choice of conductivity values, suggesting that simplified physical  
232 representations may further amplify the impact of parameter uncertainty.

233 Williams and Maxwell (2011), using coupled PF-WRF simulations, further explored the  
234 feedbacks of geological conditions on land–atmosphere processes such as latent heat flux and  
235 wind speed. Based on idealized scenarios, they conducted ensemble simulations by perturbing  
236 the hydraulic conductivity field. The results showed that conditioning the hydraulic conductivity  
237 significantly reduced uncertainties in simulating land–atmosphere interactions compared to  
238 unconditioned cases. The ensemble mean was closer to the control scenario; for instance, the  
239 mean and distribution of simulated wind speed showed reduced uncertainty. These findings  
240 provide important implications for various wind energy applications.

241 Community-wide studies have also highlighted the importance of representing water-table  
242 dynamics within land-surface processes. Koirala et al. (2014) incorporated groundwater  
243 fluctuations into the MATSIRO land surface scheme and quantified the sensitivity of ET to  
244 capillary rise, showing that global mean ET increases by approximately 9% when water-table  
245 dynamics are included. Tian et al. (2012) further examined how hydraulic conductivities  
246 regulate ET by influencing both vertical and lateral groundwater fluxes, using a coupled  
247 AquiferFlow–SiB2 modeling framework. Using ParFlow-based coupled models, Tai et al. (2018)  
248 and Fang et al. (2022) demonstrated that explicitly resolving water-table dynamics helps explain  
249 mechanisms of plant mortality, while Abbaszadeh et al. (2025) reported improved simulations  
250 of land-surface fluxes when groundwater processes are represented. Miguez-Macho and Fan  
251 (2025) incorporated lateral surface-water and groundwater subsidies simulated by the ASAP  
252 model into a humidity index, providing a more accurate depiction of the timing and magnitude  
253 of water availability in hydrologically convergent lowlands. This enhancement better explains  
254 the monthly variations of leaf area index. A more recent study (Vogelbacher et al., 2025)  
255 extends beyond physically coupled modeling frameworks by showing that integrating water-  
256 table depth into a machine-learning system yields a more robust assessment of heatwave risks.

## 257 **2.2 The critical zone of WTD in groundwater–land interactions**

258 As discussed above, numerous studies have revealed feedbacks of groundwater on land–  
259 atmosphere processes. A key scientific question thus arises: what is the quantitative  
260 relationship between land surface states/fluxes and the WTD? Maxwell and Condon (2016), in  
261 their study over the continental US, confirmed the critical role of lateral groundwater flow in  
262 modulating the partitioning between evaporation (E) and transpiration (T). This influence is most  
263 pronounced when the WTD lies between 0.5 and 5 m. Shallower WTD leads to elevated bare-  
264 soil evaporation and transpiration, while deeper WTD suppresses both fluxes. Notably, in  
265 regions where bare-soil evaporation is limited and transpiration is sustained, the T/E ratio peaks.

266 Similarly, many studies using PF-CLM have identified a critical WTD range within which  
267 land surface variables—such as latent heat flux, sensible heat flux, and surface temperature—  
268 are highly sensitive to WTD but exhibit diminished sensitivity beyond this range (Figure 1). For

Deleted: ¶

270 instance, Ferguson's work over the Little Washita watershed suggests a critical WTD range of  
271 approximately 1–10 m (Ferguson and Maxwell, 2012, 2011, 2010), while Yang et al. (2020);  
272 Yang et al. (2023) reported comparable results over the North China Plain. Rihani et al. (2015)  
273 also illustrate the coupling between WTD and planetary boundary layer depth in this transition  
274 zone from ridges to valleys along hillslopes. Fang et al. (2022) demonstrated a clear transition  
275 from hydraulic-failure-dominated mortality at shallow WTDs (<5 m) to carbon-starvation-  
276 dominated mortality under deep water-table conditions (>7.5–15 m). Generally, when WTD is  
277 shallower than this range, soil is nearly saturated and energy availability becomes the limiting  
278 factor, weakening the sensitivity of surface states/fluxes to WTD. Conversely, when WTD  
279 exceeds this range, gravity-driven drainage dominates, limiting moisture availability and again  
280 reducing sensitivity. The upper bound of this range is typically <1 m, while the lower bound  
281 often aligns with the model's coupling depth (Kollet and Maxwell, 2008). However, in some  
282 cases, such as Maxwell and Condon (2016), the lower bound extends beyond the nominal 2 m  
283 coupling depth, likely due to capillary rise from the water table.

284 This critical WTD range varies across regions, influenced by differences in subsurface  
285 characteristics and rooting depth, though current understanding remains limited. Fan et al.  
286 (2017), through analysis of over 2,200 global root depth observations and model-based  
287 inversion, showed that rooting depth is regulated by the capillary rise zone. Even within the  
288 same species and climate, rooting depth may vary with WTD conditions. (Cannon, 1913). In  
289 some environments, vegetation develops both shallow fibrous roots and deep taproots to  
290 access water under varying conditions—shallow roots for near-surface moisture during wet  
291 periods, and deep roots for capillary water during droughts. On well-drained uplands, rooting  
292 depth is controlled by infiltration and may not reach significant depths. (Sperry and Hacke, 2002;  
293 Schenk and Jackson, 2005; Xu and Li, 2008). In contrast, in shallow groundwater zones,  
294 oxygen stress may inhibit root growth and decouple vegetation from groundwater. (Wagg, 1967;  
295 Follett et al., 1974; Martin, 1968; Armstrong et al., 1976). This adaptive rooting strategy  
296 suggests that in natural systems, the depth and intensity of groundwater–land surface coupling  
297 may exceed what models typically simulate.

298 Maxwell et al. (2007) further investigated how groundwater feedbacks on land surface  
299 processes change under different climate change scenarios, including hot, hot and dry, and hot  
300 and wet. It is not difficult to infer that changes in latent heat flux and recharge (precipitation  
301 minus ET) within the critical WTD range exhibit strongest spatial variability. Generally, these  
302 findings suggest that groundwater feedbacks on land surface processes are closely linked to  
303 topographic and climatic conditions. For instance, in the aforementioned mountainous regions  
304 of Colorado, spatial variability in WTD leads to diverse groundwater–land surface interactions.  
305 The transitional zones between ridges and valleys are often the key areas for such interactions.  
306 In humid regions, the water table often follows surface topography (Gleeson et al., 2011),  
307 facilitating strong groundwater–land surface coupling. However, in arid regions, WTD may  
308 exceed the lower bound of the critical range, reducing the significance of groundwater

Formatted: Highlight

Formatted: Not Highlight

Formatted: Not Highlight

309 feedbacks. In natural systems, this interaction is often governed by the complex interplay  
310 between climate, topography, geology, and vegetation.

### 311 **2.3 The impacts of land cover and climate changes on groundwater**

312 Climate change has exacerbated mountain pine beetle infestations, leading to widespread  
313 tree mortality in the Rocky Mountains (Bearup et al., 2014). Mikkelsen et al. (2013) studied the  
314 impacts of beetle-induced forest dieback on water and energy balances at the hillslope scale  
315 using PF-CLM simulations. An idealized hillslope model (500 m × 1000 m × 12.5 m) was used,  
316 with scenarios representing different stages of infestation—green, red, grey, and dieback—by  
317 modifying the leaf area index and stomatal conductance. Simulation results showed similar  
318 levels of ET across all scenarios in winter, but significantly higher ET in summer under the  
319 green scenario, primarily due to transpiration. In contrast, the other scenarios exhibited lower  
320 ET limited by soil moisture availability, with evaporation being the dominant process. The  
321 dieback scenario produced the highest peak in snow water equivalent (SWE), and reduced  
322 canopy cover allowed more solar radiation to penetrate, accelerating snowmelt. This earlier  
323 and more rapid melt resulted in earlier and higher streamflow peaks, as well as increased  
324 subsurface storage. A related particle tracking study (Bearup et al., 2016) further demonstrated  
325 greater groundwater contributions to streamflow during late summer.

326 Condon et al. (2020) conducted a continental-scale simulation across the United States  
327 using the PF-CLM CONUS 1.0 model (Maxwell et al., 2015) to examine groundwater responses  
328 to 1°C, 2°C, and 4°C warming scenarios. Warming was found to enhance ET, with shallow  
329 groundwater providing supplementary moisture to meet the increased demand, thereby  
330 partially mitigating land surface water stress. However, prolonged warming ultimately led to  
331 continuous groundwater depletion and a decoupling of groundwater from land surface  
332 processes. The magnitude of ET increases, and groundwater storage loss varied with WTD,  
333 with the strongest responses occurring within the previously identified critical WTD range.  
334 Overall, the humid eastern U.S. exhibited greater sensitivity to warming than the arid western  
335 regions. These findings highlight the risk of underestimating groundwater–land surface  
336 feedbacks when using simplified groundwater parameterizations in ESMS.

### 337 **2.4 Enhanced LSM functionality motivates recoupling**

338 These selected representative studies have demonstrated the critical role of groundwater  
339 in Earth system processes. Over the past two decades, CoLM—like many other LSMs—has  
340 undergone substantial development, including functional extensions, improved  
341 parameterization schemes, and the introduction of multiple alternative process representations.  
342 However, our understanding of how groundwater interacts with these additional processes—  
343 including how various parameterizations respond to and influence groundwater dynamics—  
344 remains limited. These limitations underscore the pressing need to upgrade the coupling  
345 between ParFlow and LSMs. The key scientific advances of CoLM are summarized as follows  
346 (Yuan and Dai, 2025):

347       **(1) Radiation transfer:** a three-dimensional vegetation shortwave (Yuan et al., 2014) and  
348 longwave radiation transfer scheme has been incorporated, the SNICAR snow radiation  
349 transfer scheme has been added to simulate snow albedo and radiation absorption within the  
350 snowpack, and an improved two-stream approximation scheme for vegetation radiation transfer  
351 has been provided (Yuan et al., 2017). **(2) Turbulent fluxes:** the model enhances the continuity  
352 of dynamic parameters and processes across transitions from dense to sparse vegetation.  
353 Resistance coefficients below the canopy are calculated using a profile integration method. A  
354 new turbulent exchange scheme supports multiple coexisting plant functional types (PFTs)  
355 within a three-dimensional canopy. Several soil resistance parameterizations are provided to  
356 improve surface evapotranspiration estimates. Additionally, a surface turbulent flux scheme has  
357 been introduced to account for large-eddy effects. **(3) Canopy interception and plant**  
358 **hydraulics:** the model includes multiple canopy interception schemes and a plant hydraulics  
359 module governed by Darcy's law. Different parameterizations emphasize distinct physical  
360 processes and support investigation of the evolution, drivers, and trends of interception under  
361 varying conditions. The hydraulics module replaces empirical formulations that relate plant  
362 stress to soil water potential and improves the simulation of land-atmosphere water exchange  
363 under changing environments. **(4) Leaf temperature:** A simplified one-dimensional two-big-  
364 leaf scheme has been implemented to improve the numerical stability of leaf temperature  
365 simulations. In addition, a new parameterization has been developed for leaf temperature in  
366 multi-PFT scenarios with a three-dimensional canopy structure. **(5) Other functional**  
367 **extensions:** additional modules have been developed for biogeochemistry, urban systems,  
368 crop modeling, land use and land cover change, wildfire, ozone-related ecophysiological stress,  
369 and integrated hydrological processes.

### 370 **3. Foundational step toward sustainable coupling**

371       To explore the feasibility of re-coupling the latest versions of ParFlow and CoLM, we  
372 conducted a preliminary integration of the two models. This effort focuses exclusively on the  
373 basic water and energy modules of CoLM and is built upon the existing ParFlow-CLM coupling  
374 interface. That means that canopy interception, snow processes, and the surface energy  
375 balance (radiation, sensible and latent heat fluxes, and ground heat flux) were enabled in the  
376 current tests, whereas other functional extensions were kept inactive. Our goal is to understand  
377 how both models have advanced over the past two decades, in terms of functionality, code  
378 architecture (e.g., parallelism), data structures, I/O interfaces, and pre-/post-processing tools.  
379 This process also helps identify key variables and processes—along with their implementation  
380 in code—that are critical for a more comprehensive coupling effort. Although this re-coupling  
381 effort uses CoLM as an example, the experience and insights gained are also applicable to  
382 coupling ParFlow with other LSMs.

383       This initial re-coupling serves to evaluate model performance with respect to physical  
384 processes, particularly highlighting potential improvements gained through two decades of  
385 development. It also establishes a set of benchmarks for testing and debugging as more CoLM

386 modules are progressively incorporated. Without this incremental approach, the complexity of  
387 multiple physical processes would make testing and debugging considerably challenging. In  
388 addition, we fully leverage the lessons learned through trial and error over the past twenty years  
389 to ensure a more stable execution of the coupled model (Ferguson et al., 2016). While this  
390 phase emphasizes gaining a deeper understanding of the physical processes, future work on  
391 sustainable coupling will likely shift toward technical aspects—such as refining the coupling  
392 interface, improving modularity, and ensuring long-term maintainability. These efforts will  
393 collectively inform our understanding of the challenges and opportunities involved in  
394 establishing a sustainable coupling framework.

### 395 **3.1 Model setup, experimental design, and evaluation data**

396 The modeling domain, selected from the CONCN domain (Yang et al., 2025), is located in  
397 the North Pearl River Basin (Figure 2). This area was chosen as it serves as a demonstration  
398 area for the CONCN model and possesses more complete infrastructure e.g., the processed  
399 ERA5-Land reanalysis data (Muñoz-Sabater et al., 2021). To link the study domain with the  
400 coupled modeling framework, we next describe the model's vertical and horizontal  
401 discretization. Since the CONCN model and CoLM use four and ten soil layers, respectively,  
402 the CONCN model structure was adjusted to align with CoLM's vertical discretization. The  
403 ParFlow model employed in this study comprises 11 layers: the top 10 layers match CoLM in  
404 thickness, while the additional 11th layer represents the deep aquifer. ParFlow and CoLM are  
405 coupled through the top 10 layers. The coupled model maintains a horizontal resolution of ~1  
406 km, consistent with the CONCN model and includes 252 and 146 grid cells in the  $x$  and  $y$   
407 directions, respectively. This corresponds to a spatial extent of approximately 242.35 km ( $x$   
408 *direction*)  $\times$  140.41 km ( $y$  *direction*)  $\times$  103.43 m ( $z$  *direction*). Soil properties for CoLM inputs  
409 were derived from the Global Soil Dataset for Earth System Modeling (GSDE) (Shangguan et  
410 al., 2014). Soil parameters for ParFlow were reconstructed based on the sand and clay weight  
411 percentages from the same GSDE dataset, following the USDA soil classification system.  
412 Properties for the 11th layer were obtained from GLHYMPS 1.0 (Gleeson et al., 2011; Gleeson  
413 et al., 2014), as used in the CONCN model. The  $e$ -folding of aquifer hydraulic conductivity with  
414 depth was implemented using a characteristic depth of 50 m (Fan et al., 2007). Other surface  
415 input parameters—including Manning's roughness coefficients, topographic slopes, and land  
416 cover types—were adopted directly from the CONCN model configuration (Yang et al., 2025).

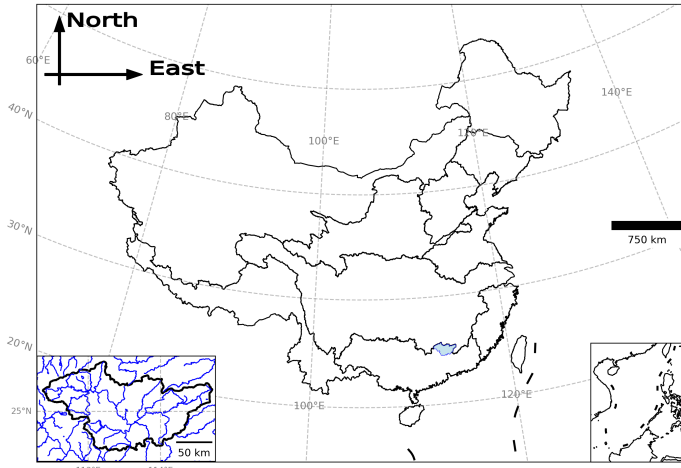


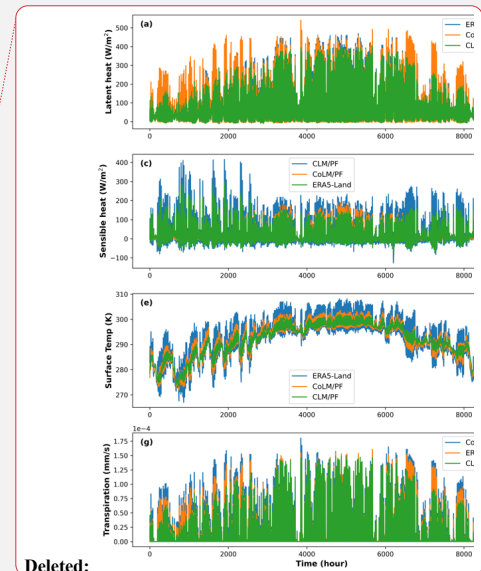
**Figure 2. Location of the modeling domain**

417  
418

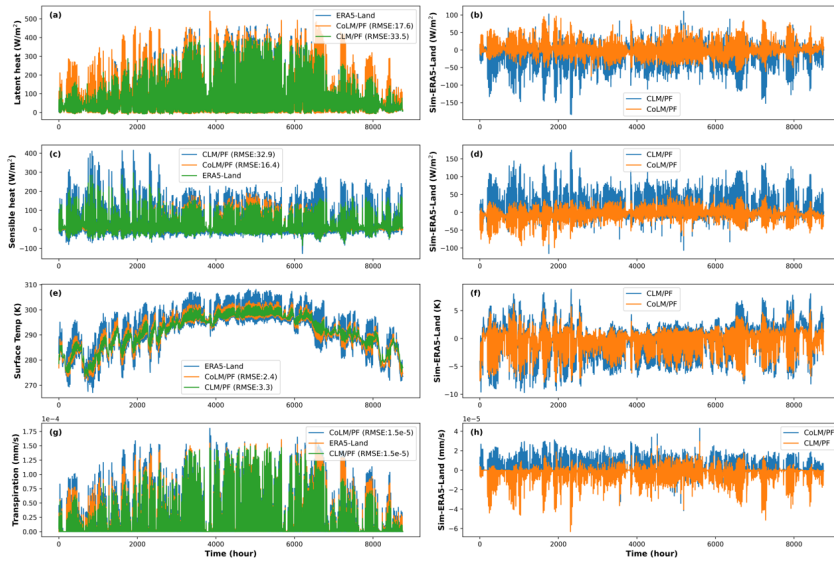
419 We first spun up the standalone ParFlow model using potential recharge data clipped from  
420 the CONCN domain. Then we drove the coupled model using the 2018 meteorological forcing  
421 from ERA5-Land reanalysis. Year 2018 was selected to keep consistency with the evaluation  
422 year of the CONCN model. However, this is an area with limited snow. To demonstrate snow  
423 performance, we created a synthetic case by applying the water year 2003 forcing from a  
424 station (Defnet et al., 2024) located in Colorado to a single column model. To evaluate changes  
425 in model performance, we also constructed 11-layer models (with 10 coupled layers) using the  
426 old ParFlow-CLM for both real-world and synthetic cases. For the real-world case, we  
427 compared the simulated sensible heat, latent heat, skin temperature, transpiration, SWE, and  
428 the water flux exchange between the new and old models (Figures 3 and 4). Here, water flux  
429 exchange refers to the source/sink terms in Richards' equation: positive values represent  
430 infiltration, while negative values are caused by ET. We also evaluated the simulation  
431 performance of the first four variables using ERA5-Land reanalysis. For the synthetic cases,  
432 we used data from the Snow Telemetry (SNOTEL) network maintained by the Natural  
433 Resources Conservation Service (NRCS)—specifically, the measured SWE at the same  
434 location as the meteorological forcing—to evaluate the models' overall ability to simulate the  
435 timing and magnitude of snowpack.

436

Deleted: W

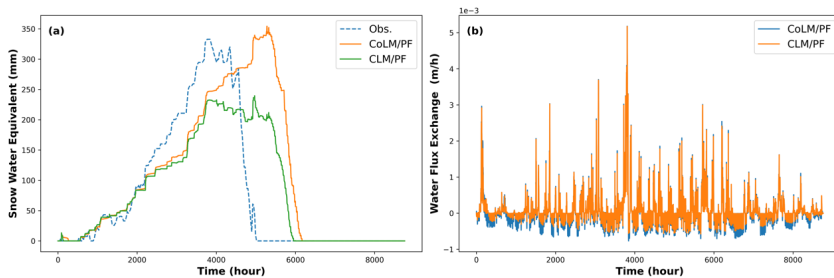


Deleted:



439  
 440 **Figure 3.** Comparison of latent heat flux, sensible heat flux, surface temperature, and  
 441 transpiration between the old CLM/ParFlow and the new CoLM/ParFlow models. The  
 442 corresponding values from ERA5-Land are plotted in the left column for reference. The  
 443 right column shows the differences between the model simulations and ERA5-Land for  
 444 each variable. Each subplot represents spatial averages over the entire modeling  
 445 domain. For clarity and to prevent overlapping, the plotting order is intentionally varied  
 446 across subplots.

447

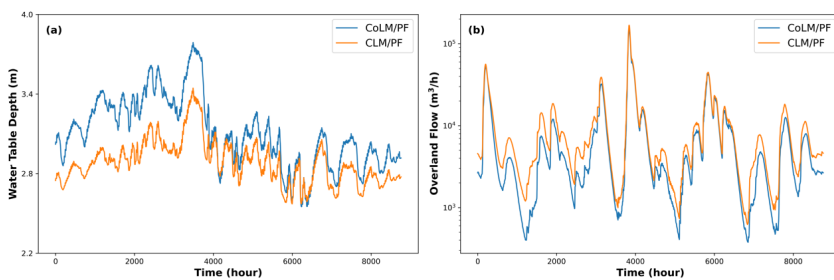


448  
 449 **Figure 4.** (a) shows the simulated snow water equivalent from the CoLM/ParFlow and  
 450 CLM/ParFlow single column models, compared against SNOTEL observations. (b)  
 451 presents the spatially averaged net water fluxes from CoLM and CLM to ParFlow,  
 452 representing the source and sink terms in the ParFlow domain; both fluxes represent  
 453 spatial averages over the entire modeling domain.

454 **3.2 Performance gains from updated CoLM support recoupling**

455 Simulations of all variables by CoLM/PF exhibit improved performance relative to CLM/PF  
 456 when evaluated against ERA5-Land reanalysis data (Figure 3). CoLM/PF produces a more  
 457 realistic partitioning of turbulent fluxes, characterized by increased latent heat and reduced  
 458 sensible heat (Figures 3a and 3c). Notably, transpiration simulated by CoLM/PF is substantially  
 459 higher and aligns more closely with ERA5-Land data (Figure 3g). Additionally, CoLM/PF more

460 accurately reproduces the fluctuations in land surface temperature compared to CLM/PF  
 461 (Figure 3e). In the single column simulations (Figure 4a), CoLM/PF also generates a higher  
 462 peak SWE than CLM/PF, showing better agreement with SNOTEL observations, although both  
 463 models display deviations in the timing of SWE accumulation. This discrepancy may stem from  
 464 the idealized subsurface configurations used in both models. Improvements in both  
 465 transpiration and SWE are further supported by previous research; for instance, O'Neill et al.  
 466 (2021) reported consistently lower ET and SWE from CLM/PF in the assessment of CONUS  
 467 1.0 model. The overall advancement in model performance can likely be attributed to the more  
 468 sophisticated process representations embedded in CoLM.



469 **Figure 5. (a) and (b) show the simulated water table depth and overland flow by**  
 470 **CoLM/ParFlow and CLM/ParFlow, respectively. Each subplot represents spatial**  
 471 **averages over the entire modeling domain.**  
 472

473 Figure 4b illustrates the net fluxes transferred from the land surface to the subsurface,  
 474 which directly influence hydrologic dynamics such as WTD and overland flow. These exchange  
 475 fluxes show greater variability in the CoLM/PF simulation, suggesting more dynamic surface–  
 476 subsurface interactions. Consistent with this, Figure 5 reveals more pronounced temporal  
 477 variability in both WTD and overland flow. A generally deeper water table is observed in  
 478 CoLM/PF (Figure 5a), which is likely a result of the higher plant water uptake, i.e., increased  
 479 transpiration, depicted in Figures 3a, 3g and 4b. Consequently, the reduction in baseflow from  
 480 groundwater may explain the observed decrease in low levels of overland flow (Figure 5b).

481 To improve the representation of turbulent exchanges between the vegetation canopy and  
 482 the atmosphere, the model employs a profile-integrated approach to resolve key dynamical  
 483 parameters (e.g., turbulent diffusivity  $K(z)$ ) with explicit vertical resolution (Dai et al., 2019b). In  
 484 particular, resistance-related variables—such as displacement height ( $d$ ) and roughness length  
 485 ( $z_0$ ), which characterize canopy-atmosphere momentum exchange, as well as aerodynamic  
 486 resistances for leaves ( $r_b$ ) and ground surface ( $r_d$ ), which govern within-canopy and near-  
 487 surface heat and vapor transfer—are refined to account for structural heterogeneity (Dai et al.,  
 488 2019b). Meanwhile, profile-integrated functions are dynamically computed based on vegetation  
 489 structure and atmospheric stability, and directly determine resistance terms (e.g.,  $r_{ah}$ ,  $r_{aw}$ ) (Yuan  
 490 and Dai, 2025). This also includes revised roughness length formulations that explicitly account  
 491 for atmospheric stability (Yuan and Dai, 2025), extending beyond the original neutral-based  
 492 assumptions in schemes such as Raupach (1994, 1992). This combined approach yields a

Formatted: Highlight

Formatted: Highlight

Formatted: Highlight

Formatted: Highlight

493 more physically consistent and vertically continuous treatment of turbulent fluxes under non-  
494 neutral stratification, enhancing realism in complex canopy conditions.

495 In addition, other schemes—such as those related to soil thermal parameters (including  
496 heat capacity and heat conductivity), as well as soil color and associated reflectance—also  
497 differ between the CoLM/PF and CLM/PF models (Yuan and Dai, 2025). All of these differences  
498 motivate a coupled model intercomparison project to evaluate how different schemes, either  
499 within a single model or across different models, affect the performance of the coupled model  
500 and land–hydrology process interactions. Since 2005, ParFlow has also undergone several  
501 major developments that significantly affect model performance (Kuffour et al., 2020), such as  
502 the integration of overland flow (Kollet and Maxwell, 2006) and the implementation of the  
503 terrain-following grid (Maxwell, 2013). Both test cases in this study already used these modern  
504 capabilities. Features such as GPU acceleration (Hokkanen et al., 2021) and reservoir  
505 capabilities (West et al., 2025) in ParFlow exist, but they are not relevant to the test cases here.

506 In this initial coupling process, we found that the main changes in CoLM were related to  
507 data structure, module organization, module names, and variable naming conventions. For  
508 example, structures were broken down into multiple arrays, modules were split and reorganized  
509 based on functionality, some modules were removed from the main program and used as  
510 preprocessing components, and module adjustments were often accompanied by renaming. A  
511 large number of variable names were also changed. Moreover, the inclusion of multiple  
512 parameterization schemes has increased code complexity to some extent, resulting in  
513 significantly larger module sizes. Nevertheless, most physical processes have retained their  
514 original core parameterizations. This means that the primary task in this initial coupling stage  
515 is to identify the key physical processes and the critical variables within the new system  
516 structure. Several new parameterization schemes have also been implemented—for example,  
517 those associated with the turbulent exchange discussed above—though the application of other  
518 schemes will require further testing in future work.

#### 519 **4. A sustainable recoupling framework for future development**

520 Here, we propose a sustainable framework for future CoLM/ParFlow coupling based on  
521 our preliminary work (Figure 6). This framework consists of four key components: a coupler-  
522 based architecture, a robust initial foundation, protocols for scalable upgrades, and a  
523 community interaction platform. The four components play different roles. The first two—  
524 coupler-based architecture and early-stage grid/process mapping—form the structural  
525 foundation that determines long-term sustainability. They address issues that cannot be solved  
526 through implementation refinements alone, such as maintaining independent model evolution  
527 and enabling robust cross-grid exchanges. The latter two components—developer protocols  
528 and community interaction—further enhance maintainability and extensibility once the  
529 structural basis is in place. These collaborative conventions support scalable development but  
530 cannot replace the structural requirements themselves, nor can they reduce the inherent

531 [complexity of multi-model coupling. Effective participation still requires sufficient domain](#)  
532 [knowledge and technical expertise.](#)

533 

- **Coupler-based architecture for long-term sustainability**

534 While the current ParFlow-Land interface built in ParFlow supports efficient coupling with  
535 land surface and atmospheric models, demonstrates good parallel performance, and avoids  
536 the overhead associated with inter-model communication, it lacks compatibility with  
537 standardized coupling frameworks and protocols. This limits the integration of coupled models  
538 into broader Earth system modeling frameworks. In contrast, coupler-based architectures—  
539 such as ESMF/NUOPC, CESM/cpl7, and OASIS3-MCT—are now standard in modern Earth  
540 system modeling. They preserve the native data structures, domain decomposition, and parallel  
541 logic of each model, which is particularly important given the substantial structural differences  
542 between ParFlow and CoLM. For instance, this approach allows retaining ParFlow’s GPU-  
543 based parallelism (Hokkanen et al., 2021) and CoLM’s MPI-based structure, along with their  
544 respective domain decomposition strategies. It also enables continued use of each model’s  
545 preferred data format and processing tools—for example, ParFlow’s `.pfb` format and `pftools`,  
546 as well as CoLM’s NetCDF-based workflow. Adopting a standardized coupler thus facilitates  
547 modular development, cross-system compatibility, and long-term maintainability. Looking  
548 forward, such coupler-based designs could also be extended to support surrogate model  
549 integration (Bennett et al., 2024; Tran et al., 2021), enabling hybrid workflows that combine  
550 physical models and AI-based components.

551 

- **Strong foundations through early-stage mapping**

552 Laying a solid foundation during the initial coupling phase is critical. First, a mapping  
553 between ParFlow’s grid and CoLM’s subgrids must be established to support future model  
554 extensions. The current coupling only supports integration based on the LCT (Land Cover Type)  
555 subgrid, whereas important functional extensions such as biogeochemistry and 3D vegetation  
556 canopy processes rely on plant function types (PFTs) and the associated PFT and PC (Plant  
557 Community) subgrids. The mapping between grids of different models is a key concern in the  
558 coupling community and directly affects coupling performance (Valcke, 2022). Currently, most  
559 approaches rely on physical interpolation methods; incorporating an AI-based scale  
560 transformation layer with mass conservation constraints could be a promising enhancement.  
561 Second, key variables and processes from newly introduced modules or previously untested  
562 parameterizations must be identified. For example, the plant hydraulics module requires soil  
563 hydraulic conductivity fields, which are not included in the current coupling interface. More  
564 importantly, a structured logging system should be implemented to track all exchanged  
565 variables, their associated modules, and the corresponding grid structures, thereby ensuring  
566 transparency and traceability throughout development. [This logging mechanism differs from](#)  
567 [conventional version-control systems in that it records the evolution of coupling-relevant](#)  
568 [variables and grid mappings rather than general code revisions, providing scientific rather than](#)  
569 [software-level traceability.](#)

570 • **Protocols for efficient and maintainable coupler upgrades**

571 Two key aspects are emphasized. First, the architecture of interfaces and coupling layers  
572 should be designed for long-term clarity and ease of maintenance. Taking ESMF/NUOPC as  
573 an example, the model-side interfaces and coupler-side connector and mediator layers are  
574 implemented with a focus on modular organization, encapsulated data exchange, and well-  
575 structured control flow, ensuring that the system can be reliably extended as new model  
576 features or physical processes are introduced. For example, TerrSysMP achieves good  
577 modularity by separating tasks such as sending/receiving fields, grid mapping, and variable  
578 registration into dedicated files (Shrestha et al., 2014). TerrSysMP2 further improves on this  
579 design by organizing these components within a single Fortran module, which makes the  
580 interface structure clearer and simplifies the CMake build process (Poll et al., 2024). Second,  
581 developers introducing new modules, parallelization strategies, or grid structures, within one  
582 model must explicitly assess their potential impact on the other model, clarify any newly  
583 introduced variables or data structures to be exchanged via the coupler, and submit pull  
584 requests with corresponding explanations. Senior maintainers should review these changes  
585 and provide targeted feedback on necessary updates to the interface and coupling logic. All  
586 modifications affecting model interaction must be tracked in the logging system described  
587 above, and no update should be considered complete until it is formally registered in the log.

588 • **Community platform for collaboration and maintenance**

589 A dedicated community platform—such as a GitHub repository, mailing list, or model  
590 portal—should be established to support developer–user interaction, technical discussion, and  
591 feedback collection. This platform will also serve to announce new model releases, coupling  
592 layer updates, or changes in the logging system. Transparent communication and community-  
593 driven collaboration are essential for the long-term sustainability and extensibility of the coupled  
594 model system. Looking forward, we envision extending this platform into a broader, community-  
595 driven environment for managing and operating ParFlow–LSM coupled models, drawing  
596 inspiration from efforts such as eWaterCycle (Hut et al., 2022). Beyond supporting collaboration  
597 and information sharing, such a platform could streamline model configuration, coupled-model  
598 execution, workflows, data processing/formatting, and reproducibility—thereby accelerating  
599 adoption, improving transparency, and fostering interoperability across hydrological and Earth  
600 system science communities. This would also address a current gap, as ParFlow-based  
601 coupled systems remain largely fragmented and lack standardized tools for interfacing with  
602 upstream/downstream models, verification and benchmarking, and public release to users.

- Deleted: ing
- Deleted: exchange
- Deleted: ,
- Deleted: integration
- Deleted:
- Deleted: integration
- Deleted: testing
- Deleted: dissemination

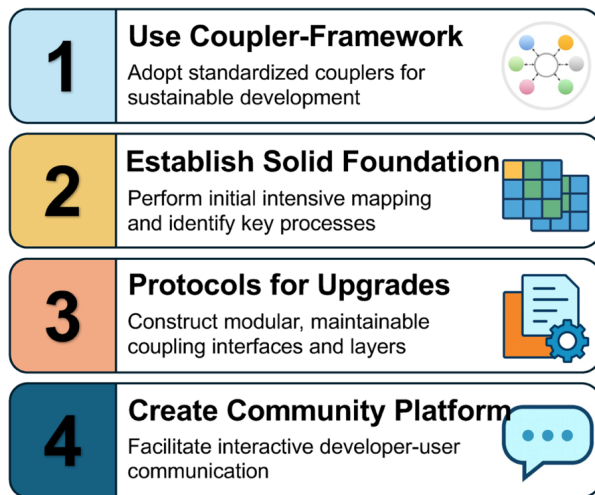


Figure 6. The coupling framework for sustainable development

#### 5. ParFlow-Land coupled model intercomparison project (PLCMIP)

Over the past decades, numerous land and/or atmosphere models coupled with ParFlow have been developed (Table 1). These models vary in their functional capabilities and adopt different coupling strategies, which may significantly affect computational efficiency. The two models coupled with CoLM aim to understand the fundamental interactions of water and energy between subsurface and land surface processes (Dai et al., 2003; Maxwell and Miller, 2005). In contrast, the two models coupled with ARPS and WRF (Maxwell et al., 2007; Maxwell et al., 2011; Skamarock and Klemp, 2008; Xue et al., 2000; Xue et al., 2001), along with the two generations of TerrSysMP (Shrestha et al., 2014; Oleson et al., 2008; Lawrence et al., 2019; Poll et al., 2024), provide capabilities to explore two-way feedbacks across each interface within the subsurface–land surface–atmosphere system. Furthermore, the coupling of ParFlow with TREES (Tai et al., 2018; Mackay et al., 2015), ELM-FATES (Fang et al., 2022; Caldwell et al., 2019; Fisher et al., 2015; Leung et al., 2020), and LPJ-GUESS (Jia et al., 2025) introduces advanced vegetation dynamics into land surface process representations. Finally, integration with NASA-LIS enables data assimilation within the coupled modeling framework (Maina et al., 2025; Kumar et al., 2008; Niu et al., 2011; Abbaszadeh et al., 2025), and TerrSysMP also incorporates the PDAF (Parallel Data Assimilation Framework) to support data assimilation capabilities (Kurtz et al., 2016). Overall, most of the ParFlow-based coupled systems are implemented through modular integration—embedding one model within another—whereas TSMP and ParFlow-LIS represent coupler-based architectures that mediate data exchange among components.

Model intercomparison provides a valuable means to assess model development and foster connections or collaborations across research communities. Several well-known

Deleted: and

637 intercomparison projects exist, such as the Coupled Model Intercomparison Project (CMIP) for  
 638 ESM intercomparison (Eyring et al., 2016), and the Land Surface, Snow and Soil Moisture  
 639 Model Intercomparison Project (LS3MIP) (Van Den Hurk et al., 2016), which is designed to  
 640 assess the performance of land modules in current ESMs. In addition, individual  
 641 intercomparison activities have also been widely conducted within the land surface modeling  
 642 community (Scanlon et al., 2018; Liu et al., 2023). ParFlow has also participated in various  
 643 model intercomparison projects involving hydrologic models and an increasing number of  
 644 individual modeling studies, such as those by Maxwell et al. (2014); Sulis et al. (2017); Kollet  
 645 et al. (2017); Sulis et al. (2010). Given the differences among the ParFlow-based coupled  
 646 models mentioned above, a dedicated model intercomparison project (MIP) is needed to  
 647 systematically evaluate coupled models and support the development of a community platform  
 648 for benchmarking and collaboration, with the following objectives:

- 649 • To quantify the strength and spatiotemporal variability of groundwater–land–  
 650 atmosphere interactions resulting from different parameterization schemes used in  
 651 various land surface and atmospheric models.
- 652 • To evaluate the parameter sensitivity of each scheme, ensuring that differences\*  
 653 attributed to model structure are not confounded with parameter choices.
- 654 • To compare computational efficiency across different coupling strategies.
- 655 • To identify the unique functionalities and strengths of each coupled model, providing  
 656 users with guidance in selecting the most appropriate model for their specific research  
 657 needs.

658 To ensure meaningful and comparable evaluations across models, the PLCMIP will\*  
 659 encourage the use of standardized benchmark cases—either synthetic experiments or a  
 660 common real-world watershed—as well as unified datasets for parameters and meteorological  
 661 forcing. In addition, other groundwater-land coupled models, as well as land surface models  
 662 with improved groundwater parameterizations, are likewise encouraged to participate in this  
 663 intercomparison effort. Representative examples include, Shen et al. (2016); Zeng et al. (2018);  
 664 Tian et al. (2012); Niu et al. (2014); Sutanudjaja et al. (2014); Liao et al. (2025); Miguez-Macho  
 665 and Fan (2025); Akhter et al. (2025); Dai et al. (2019a), although participation in PLCMIP is not  
 666 limited to these.

667 **6. Summary**

668 Twenty years after the original ParFlow-CLM coupling (Maxwell and Miller, 2005), this study  
 669 reaffirms the long-term scientific and technical significance of that foundational effort. Over two  
 670 decades, the coupled system has made major contributions in establishing the critical role of  
 671 groundwater in modulating subsurface–land–atmosphere feedbacks and identifying the  
 672 existence of a critical water table depth range that governs these bidirectional interactions.  
 673 Technically, this coupling demonstrated a viable approach for integrating a groundwater model  
 674 with a land surface scheme—the lower boundary of Earth system models—thereby providing  
 675 a template for incorporating groundwater processes into ESMs. To revisit and update this

Deleted: (1)  
 Formatted: Font: (Asian) Arial Unicode MS

Formatted: Font: (Default) Arial, (Asian) Arial Unicode MS, 10 pt, Not Bold

Formatted: List Paragraph, Bulleted + Level: 1 + Aligned at: 0.25" + Indent at: 0.5"

Formatted: Font: (Asian) Arial Unicode MS

Deleted: (2)

Deleted: (3)

Formatted: Font: (Default) Arial, (Asian) Arial Unicode MS, 10 pt, Not Bold

Formatted: Font: (Default) Arial, (Asian) Arial Unicode MS, 10 pt, Not Bold

Formatted: Tab stops: Not at 0.5"

Formatted: Not Highlight

Formatted: Not Highlight

Formatted: Not Highlight

Formatted: Font: (Asian) Arial Unicode MS

679 legacy, we carried out a preliminary re-coupling of the latest versions of ParFlow and CoLM,  
680 focusing on core water and energy processes. This re-coupling already reveals improved model  
681 performance and provides a functional platform for incremental expansion and benchmarking.

682 Looking ahead, several key steps are essential for advancing a sustainable and extensible  
683 ParFlow–LSM coupling framework. Achieving this vision will require a more comprehensive  
684 and community-oriented design. This includes adopting a lightweight coupler architecture that  
685 preserves each model's native data structures, parallel strategies, and processing tools, while  
686 supporting modular integration of new physical or surrogate components. To ensure long-term  
687 maintainability and usability, we also envision a community platform that unifies model  
688 configuration, user workflows, and benchmarking functions. Such a platform would enhance  
689 transparency, reproducibility, and ease of adoption across the hydrologic and Earth system  
690 modeling communities. In parallel, we propose launching a model intercomparison project  
691 (PLCMIP) to systematically evaluate performance, compare coupling strategies, and guide  
692 future development.

693

694

Deleted: Looking forward, d

Deleted: eveloping a sustainable ParFlow–LSM coupling framework

Deleted: support

Deleted: shared

Deleted: integrates

Deleted: coupling

Deleted: data exchange,

Table 1. ParFlow and Land/Atmosphere coupled models

Coupled model	Model description	Coupling approach	Reference
CoLM	The Common Land Model	CoLM as a subroutine	<b>Maxwell and Miller, 2005;</b> Dai et al., 2003
ARPS	The mesoscale atmospheric model Advanced Regional Prediction System; coupled with the built-in land surface model	ARPS as a subroutine	<b>Maxwell et al., 2007;</b> Xue et al., 2000, 2001
WRF	The community numerical weather prediction Weather Research and Forecasting model, version 3.0; coupled with the built-in Noah model	WRF as a subroutine	<b>Maxwell et al., 2011;</b> Skamarock and Klemp, 2008
CLM3.5	The NCAR Community Land Model (version 3.5) in TerrSysMP	<b>Coupler.</b> Ocean Atmosphere Sea Ice Soil, version 3.0 (OASIS3)	<b>Shrestha et al., 2014;</b> Oleson et al., 2008
TREES	A plant physiology model: Terrestrial Regional Ecosystem Exchange Simulator	TREES as a subroutine	<b>Tai et al., 2018;</b> Mackay et al., 2015
ELM	The Energy Exascale Earth System Model (E3SM) land model (ELM) that includes the Functionally Assembled Terrestrial Ecosystem Simulator (FATES)	ParFlow as a subroutine	<b>Fang et al., 2022;</b> Caldwell et al., 2019; Leung et al., 2020; Fisher et al., 2015
eCLM	An adaption of the NCAR Community Land Model (version 5.0) in TerrSysMP2	<b>Coupler.</b> OASIS3-MCT, where MCT represents Model Coupling Toolkit	<b>Poll et al., 2024;</b> Lawrence et al., 2019
Noah-MP	Noah-MP in the NASA Land Information System (LIS)	<b>Coupler.</b> The Earth System Modeling Framework and the National United Operational Prediction Capability (ESMF/NUOPC)	<b>Maina et al., 2025;</b> <a href="#">Abbaszadeh et al., 2025</a> ; Kumar et al., 2008; Niu et al., 2011
<a href="#">LPJ-GUESS</a>	<a href="#">A process-based dynamic vegetation-terrestrial ecosystem model</a>	<b>Coupler.</b> <a href="#">In-house developed</a>	<b>Jia et al. (2025)</b>
CoLM2024	The Common Land Model, version 2024	CoLM2024 as a subroutine	<b>This study</b>

Formatted: Font: Not Bold

705 **Code and data availability**

706 The datasets used in this study are all from public sources and are cited in the main text.  
707 ParFlow version 3.13, as used in this study, is available at  
708 <https://doi.org/10.5281/zenodo.4816884> (Smith et al., 2024). The new ParFlow–CoLM model  
709 and the test cases, including input and output files, are available at  
710 <https://doi.org/10.5281/zenodo.16879407> (Yang, 2025), and a copy is also available on GitHub  
711 at <https://github.com/aureliayang/parflow-colm>.

712 **Author contributions**

713 Conceptualization: CY and RM. Methodology: CY, YD, and RM. Investigation: CY, AS, SZ,  
714 YD, SK, and RM. Resources: CY, YD, and RM. Writing (original draft): CY. Writing (review and  
715 editing): CY, YD, SK, and RM.

716 **Competing interests**

717 The contact author has declared that none of the authors has any competing interests.

718 **Acknowledgements**

719 We gratefully acknowledge that the work reported in this paper was largely performed using  
720 the Princeton Research Computing resources at Princeton University, made up of a consortium  
721 of groups led by the Princeton Institute for Computational Science and Engineering (PICSciE)  
722 and the Office of Information Technology's Research Computing.

723

724 **References**

- 725 Abbaszadeh, P., Zaouna Maina, F., Yang, C., Rosen, D., Kumar, S., Rodell, M., and Maxwell, R.: Coupling  
726 the ParFlow Integrated Hydrology Model within the NASA Land Information System: a case study over  
727 the Upper Colorado River Basin, *Hydrol. Earth Syst. Sci.*, 29, 5429-5452, 10.5194/hess-29-5429-2025,  
728 2025.
- 729 Akhter, T., Pokhrel, Y., Felfelani, F., Ducharne, A., Lo, M.-H., and Reinecke, R.: Implications of Lateral  
730 Groundwater Flow Across Varying Spatial Resolutions in Global Land Surface Modeling, *Water Resour*  
731 *Res*, 61, e2024WR038523, <https://doi.org/10.1029/2024WR038523>, 2025.
- 732 Armstrong, W., Booth, T. C., Priestley, P., and Read, D. J.: The Relationship Between Soil Aeration,  
733 Stability and Growth of Sitka Spruce (*Picea sitchensis* (Bong.) Carr.) on Upland Peaty Gleys, *Journal of*  
734 *Applied Ecology*, 13, 585-591, 10.2307/2401805, 1976.
- 735 Ashby, S. F. and Falgout, R. D.: A parallel multigrid preconditioned conjugate gradient algorithm for  
736 groundwater flow simulations, *Nucl Sci Eng*, 124, 145-159, 1996.
- 737 Bearup, L. A., Maxwell, R. M., and McCray, J. E.: Hillslope response to insect-induced land-cover change:  
738 an integrated model of end-member mixing, *Ecohydrology*, 9, 195-203, 2016.
- 739 Bearup, L. A., Maxwell, R. M., Clow, D. W., and McCray, J. E.: Hydrological effects of forest transpiration  
740 loss in bark beetle-impacted watersheds, *Nat Clim Change*, 4, 481, 10.1038/nclimate2198  
741 <https://www.nature.com/articles/nclimate2198#supplementary-information>, 2014.
- 742 Bennett, A., Tran, H., De la Fuente, L., Triplett, A., Ma, Y., Melchior, P., Maxwell, R. M., and Condon, L.  
743 E.: Spatio-Temporal Machine Learning for Regional to Continental Scale Terrestrial Hydrology, *J Adv*  
744 *Model Earth Sy*, 16, e2023MS004095, <https://doi.org/10.1029/2023MS004095>, 2024.
- 745 Caldwell, P. M., Mаметjanov, A., Tang, Q., Van Roekel, L. P., Golaz, J.-C., Lin, W., Bader, D. C., Keen, N.  
746 D., Feng, Y., Jacob, R., Maltrud, M. E., Roberts, A. F., Taylor, M. A., Veneziani, M., Wang, H., Wolfe, J. D.,  
747 Balaguru, K., Cameron-Smith, P., Dong, L., Klein, S. A., Leung, L. R., Li, H.-Y., Li, Q., Liu, X., Neale, R. B.,  
748 Pinheiro, M., Qian, Y., Ullrich, P. A., Xie, S., Yang, Y., Zhang, Y., Zhang, K., and Zhou, T.: The DOE E3SM

749 Coupled Model Version 1: Description and Results at High Resolution, *J Adv Model Earth Sy*, 11, 4095-  
750 4146, <https://doi.org/10.1029/2019MS001870>, 2019.

751 Cannon, W. A.: Some Relations Between Root Characters, Ground Water and Species Distribution,  
752 *Science*, 37, 420-423, doi:10.1126/science.37.950.420, 1913.

753 Condon, L. E., Atchley, A. L., and Maxwell, R. M.: Evapotranspiration depletes groundwater under  
754 warming over the contiguous United States, *Nat Commun*, 11, 873, 10.1038/s41467-020-14688-0, 2020.

755 Dai, Y., Zhang, S., Yuan, H., and Wei, N.: Modeling Variably Saturated Flow in Stratified Soils With Explicit  
756 Tracking of Wetting Front and Water Table Locations, *Water Resour Res*, 55, 7939-7963,  
757 <https://doi.org/10.1029/2019WR025368>, 2019a.

758 Dai, Y., Yuan, H., Xin, Q., Wang, D., Shangguan, W., Zhang, S., Liu, S., and Wei, N.: Different  
759 representations of canopy structure—A large source of uncertainty in global land surface modeling,  
760 *Agricultural and Forest Meteorology*, 269-270, 119-135,  
761 <https://doi.org/10.1016/j.agrformet.2019.02.006>, 2019b.

762 Dai, Y. J., Zeng, X. B., Dickinson, R. E., Baker, I., Bonan, G. B., Bosilovich, M. G., Denning, A. S., Dirmeyer,  
763 P. A., Houser, P. R., Niu, G. Y., Oleson, K. W., Schlosser, C. A., and Yang, Z. L.: The Common Land Model,  
764 *B Am Meteorol Soc*, 84, 1013-1023, 10.1175/Bams-84-8-1013, 2003.

765 de Graaf, I. E. M. and Stahl, K.: A model comparison assessing the importance of lateral groundwater  
766 flows at the global scale, *Environ Res Lett*, 17, 2022.

767 de Graaf, I. E. M., van Beek, R. L. P. H., Gleeson, T., Moosdorf, N., Schmitz, O., Sutanudjaja, E. H., and  
768 Bierkens, M. F. P.: A global-scale two-layer transient groundwater model: Development and application  
769 to groundwater depletion, *Adv Water Resour*, 102, 53-67,  
770 <https://doi.org/10.1016/j.advwatres.2017.01.011>, 2017.

771 Defnet, A., Hasling, W., Condon, L., Johnson, A., Artavanis, G., Triplett, A., Lytle, W., and Maxwell, R.:  
772 hf\_hydrodata: A Python package for accessing hydrologic simulations and observations across the  
773 United States, *Journal of Open Source Software*, 9, 6623, 2024.

774 Eyring, V., Bony, S., Meehl, G. A., Senior, C. A., Stevens, B., Stouffer, R. J., and Taylor, K. E.: Overview of  
775 the Coupled Model Intercomparison Project Phase 6 (CMIP6) experimental design and organization,  
776 *Geosci. Model Dev.*, 9, 1937-1958, 10.5194/gmd-9-1937-2016, 2016.

777 Fan, Y., Miguez-Macho, G., Jobbágy, E. G., Jackson, R. B., and Otero-Casal, C.: Hydrologic regulation of  
778 plant rooting depth, *Proceedings of the National Academy of Sciences*, 114, 10572-10577,  
779 10.1073/pnas.1712381114, 2017.

780 Fan, Y., Miguez-Macho, G., Weaver, C. P., Walko, R., and Robock, A.: Incorporating water table  
781 dynamics in climate modeling: 1. Water table observations and equilibrium water table simulations,  
782 *Journal of Geophysical Research: Atmospheres*, 112, <https://doi.org/10.1029/2006JD008111>, 2007.

783 Fan, Y., Clark, M., Lawrence, D. M., Swenson, S., Band, L. E., Brantley, S. L., Brooks, P. D., Dietrich, W. E.,  
784 Flores, A., Grant, G., Kirchner, J. W., Mackay, D. S., McDonnell, J. J., Milly, P. C. D., Sullivan, P. L., Tague,  
785 C., Ajami, H., Chaney, N., Hartmann, A., Hazenberg, P., McNamara, J., Pelletier, J., Perket, J.,  
786 Rouholahnejad-Freund, E., Wagener, T., Zeng, X., Beighley, E., Buzan, J., Huang, M., Livneh, B., Mohanty,  
787 B. P., Nijssen, B., Saifee, M., Shen, C., van Verseveld, W., Volk, J., and Yamazaki, D.: Hillslope Hydrology  
788 in Global Change Research and Earth System Modeling, *Water Resour Res*, 55, 1737-1772,  
789 10.1029/2018wr023903, 2019.

790 Fang, Y., Leung, L. R., Koven, C. D., Bisht, G., Detto, M., Cheng, Y., McDowell, N., Muller-Landau, H.,  
791 Wright, S. J., and Chambers, J. Q.: Modeling the topographic influence on aboveground biomass using  
792 a coupled model of hillslope hydrology and ecosystem dynamics, *Geosci. Model Dev.*, 15, 7879-7901,  
793 10.5194/gmd-15-7879-2022, 2022.

794 Ferguson, I. M. and Maxwell, R. M.: Role of groundwater in watershed response and land surface  
795 feedbacks under climate change, *Water Resour Res*, 46, 2010.

796 Ferguson, I. M. and Maxwell, R. M.: Hydrologic and land-energy feedbacks of agricultural water  
797 management practices, *Environ Res Lett*, 6, ArtN 014006  
798 10.1088/1748-9326/6/1/014006, 2011.

799 Ferguson, I. M. and Maxwell, R. M.: Human impacts on terrestrial hydrology: climate change versus  
800 pumping and irrigation, *Environ Res Lett*, 7, ArtN 044022  
801 10.1088/1748-9326/7/4/044022, 2012.

802 Ferguson, I. M., Jefferson, J. L., Maxwell, R. M., and Kollet, S. J.: Effects of root water uptake formulation  
803 on simulated water and energy budgets at local and basin scales, *Environ Earth Sci*, 75, ARTN 316  
804 10.1007/s12665-015-5041-z, 2016.

805 Fisher, R. A., Muszala, S., Versteinstein, M., Lawrence, P., Xu, C., McDowell, N. G., Knox, R. G., Koven, C.,  
806 Holm, J., Rogers, B. M., Spessa, A., Lawrence, D., and Bonan, G.: Taking off the training wheels: the  
807 properties of a dynamic vegetation model without climate envelopes, *CLM4.5(ED)*, *Geosci. Model Dev.*,  
808 8, 3593-3619, 10.5194/gmd-8-3593-2015, 2015.

809 Follett, R. F., Allmaras, R. R., and Reichman, G. A.: Distribution of Corn Roots in Sandy Soil with a  
810 Declining Water Table, *Agronomy Journal*, 66, 288-292,  
811 <https://doi.org/10.2134/agronj1974.00021962006600020030x>, 1974.

812 Forrester, M. M. and Maxwell, R. M.: Impact of Lateral Groundwater Flow and Subsurface Lower  
813 Boundary Conditions on Atmospheric Boundary Layer Development over Complex Terrain, *J*  
814 *Hydrometeorol*, 21, 1133-1160, <https://doi.org/10.1175/JHM-D-19-0029.1>, 2020.

815 Gleeson, T., Marklund, L., Smith, L., and Manning, A. H.: Classifying the water table at regional to  
816 continental scales, *Geophys Res Lett*, 38, Artn L05401  
817 10.1029/2010gl046427, 2011.

818 Gleeson, T., Moosdorf, N., Hartmann, J., and van Beek, L. P. H.: A glimpse beneath earth's surface:  
819 GLoBal HYdrogeology MaPs (GLHYMPS) of permeability and porosity, *Geophys Res Lett*, 41, 3891-3898,  
820 10.1002/2014gl059856, 2014.

821 Hokkanen, J., Kollet, S., Kraus, J., Herten, A., Hrywniak, M., and Pleiter, D.: Leveraging HPC accelerator  
822 architectures with modern techniques — hydrologic modeling on GPUs with ParFlow, *Computat Geosci*,  
823 25, 1579-1590, 10.1007/s10596-021-10051-4, 2021.

824 Hut, R., Drost, N., van de Giesen, N., van Werkhoven, B., Abdollahi, B., Aerts, J., Albers, T., Alidoost, F.,  
825 Andela, B., Camphuijsen, J., Dzigian, Y., van Haren, R., Hutton, E., Kalverla, P., van Meersbergen, M., van  
826 den Oord, G., Pelupessy, I., Smeets, S., Verhoeven, S., de Vos, M., and Weel, B.: The eWaterCycle  
827 platform for open and FAIR hydrological collaboration, *Geosci. Model Dev.*, 15, 5371-5390,  
828 10.5194/gmd-15-5371-2022, 2022.

829 Ivanov, V. Y., Vivoni, E. R., Bras, R. L., and Entekhabi, D.: Catchment hydrologic response with a fully  
830 distributed triangulated irregular network model, *Water Resour Res*, 40,  
831 <https://doi.org/10.1029/2004WR003218>, 2004.

832 Jia, Z., Chen, S., Fu, Y. H., Martín Belda, D., Wärlind, D., Olin, S., Xu, C., and Tang, J.: Advancing  
833 Ecohydrological Modelling: Coupling LPJ-GUESS with ParFlow for Integrated Vegetation and Surface-  
834 Subsurface Hydrology Simulations, *EGUsphere*, 2025, 1-31, 10.5194/egusphere-2025-4064, 2025.

835 Jones, J. E. and Woodward, C. S.: Newton-Krylov-multigrid solvers for large-scale, highly heterogeneous,  
836 variably saturated flow problems, *Adv Water Resour*, 24, 763-774, Doi 10.1016/S0309-1708(00)00075-  
837 0, 2001.

838 Keune, J., Gasper, F., Goergen, K., Hense, A., Shrestha, P., Sulis, M., and Kollet, S.: Studying the influence  
839 of groundwater representations on land surface-atmosphere feedbacks during the European heat wave  
840 in 2003, *J Geophys Res-Atmos*, 121, 13301-13325, 10.1002/2016jd025426, 2016.

841 Koirala, S., Yeh, P. J.-F., Hirabayashi, Y., Kanae, S., and Oki, T.: Global-scale land surface hydrologic  
842 modeling with the representation of water table dynamics, *Journal of Geophysical Research: Atmospheres*,  
843 119, 75-89, <https://doi.org/10.1002/2013JD020398>, 2014.

844 Kollet, S., Sulis, M., Maxwell, R. M., Paniconi, C., Putti, M., Bertoldi, G., Coon, E. T., Cordano, E., Endrizzi,  
845 S., Kikinzon, E., Mouche, E., Mügler, C., Park, Y.-J., Refsgaard, J. C., Stisen, S., and Sudicky, E.: The  
846 integrated hydrologic model intercomparison project, IH-MIP2: A second set of benchmark results to  
847 diagnose integrated hydrology and feedbacks, *Water Resour Res*, 53, 867-890,  
848 <https://doi.org/10.1002/2016WR019191>, 2017.

849 Kollet, S. J. and Maxwell, R. M.: Integrated surface-groundwater flow modeling: A free-surface overland  
850 flow boundary condition in a parallel groundwater flow model, *Adv Water Resour*, 29, 945-958, 2006.

851 Kollet, S. J. and Maxwell, R. M.: Capturing the influence of groundwater dynamics on land surface  
852 processes using an integrated, distributed watershed model, *Water Resour Res*, 44, Artn W02402  
853 10.1029/2007wr006004, 2008.

854 Kuffour, B. N. O., Engdahl, N. B., Woodward, C. S., Condon, L. E., Kollet, S., and Maxwell, R. M.:  
855 Simulating coupled surface-subsurface flows with ParFlow v3.5.0: capabilities, applications, and  
856 ongoing development of an open-source, massively parallel, integrated hydrologic model, *Geosci.*  
857 *Model Dev.*, 13, 1373-1397, 10.5194/gmd-13-1373-2020, 2020.

858 Kumar, S. V., Reichle, R. H., Peters-Lidard, C. D., Koster, R. D., Zhan, X., Crow, W. T., Eylander, J. B., and  
859 Houser, P. R.: A land surface data assimilation framework using the land information system:  
860 Description and applications, *Adv Water Resour*, 31, 1419-1432,  
861 <https://doi.org/10.1016/j.advwatres.2008.01.013>, 2008.

862 Kurtz, W., He, G., Kollet, S. J., Maxwell, R. M., Vereecken, H., and Hendricks Franssen, H. J.: TerrSysMP–  
863 PDAF (version 1.0): a modular high-performance data assimilation framework for an integrated land  
864 surface–subsurface model, *Geosci. Model Dev.*, 9, 1341-1360, 10.5194/gmd-9-1341-2016, 2016.

865 Lawrence, D. M., Fisher, R. A., Koven, C. D., Oleson, K. W., Swenson, S. C., Bonan, G., Collier, N., Ghimire,  
866 B., van Kampenhout, L., Kennedy, D., Kluzek, E., Lawrence, P. J., Li, F., Li, H., Lombardozzi, D., Riley, W.  
867 J., Sacks, W. J., Shi, M., Vertenstein, M., Wieder, W. R., Xu, C., Ali, A. A., Badger, A. M., Bisht, G., van den  
868 Broeke, M., Brunke, M. A., Burns, S. P., Buzan, J., Clark, M., Craig, A., Dahlin, K., Drewniak, B., Fisher, J.  
869 B., Flanner, M., Fox, A. M., Gentine, P., Hoffman, F., Keppel-Aleks, G., Knox, R., Kumar, S., Lenaerts, J.,  
870 Leung, L. R., Lipscomb, W. H., Lu, Y., Pandey, A., Pelletier, J. D., Perket, J., Randerson, J. T., Ricciuto, D.  
871 M., Sanderson, B. M., Slater, A., Subin, Z. M., Tang, J., Thomas, R. Q., Val Martin, M., and Zeng, X.: The  
872 Community Land Model Version 5: Description of New Features, Benchmarking, and Impact of Forcing  
873 Uncertainty, *J Adv Model Earth Sy*, 11, 4245-4287, <https://doi.org/10.1029/2018MS001583>, 2019.

874 Leung, L. R., Bader, D. C., Taylor, M. A., and McCoy, R. B.: An Introduction to the E3SM Special Collection:  
875 Goals, Science Drivers, Development, and Analysis, *J Adv Model Earth Sy*, 12, e2019MS001821,  
876 <https://doi.org/10.1029/2019MS001821>, 2020.

877 Liao, C., Leung, L. R., Fang, Y., Tesfa, T., and Negron-Juarez, R.: Representing lateral groundwater flow  
878 from land to river in Earth system models, *Geosci. Model Dev.*, 18, 4601-4624, 10.5194/gmd-18-4601-  
879 2025, 2025.

880 Liu, J., Yang, Z.-L., Jia, B., Wang, L., Wang, P., Xie, Z., and Shi, C.: Elucidating Dominant Factors Affecting  
881 Land Surface Hydrological Simulations of the Community Land Model over China, *Advances in*  
882 *Atmospheric Sciences*, 40, 235-250, 10.1007/s00376-022-2091-5, 2023.

883 Mackay, D. S., Roberts, D. E., Ewers, B. E., Sperry, J. S., McDowell, N. G., and Pockman, W. T.:  
884 Interdependence of chronic hydraulic dysfunction and canopy processes can improve integrated  
885 models of tree response to drought, *Water Resour Res*, 51, 6156-6176,  
886 <https://doi.org/10.1002/2015WR017244>, 2015.

887 Maina, F. Z., Rosen, D., Abbaszadeh, P., Yang, C., Kumar, S. V., Rodell, M., and Maxwell, R.: Integrating  
888 the Interconnections Between Groundwater and Land Surface Processes Through the Coupled NASA  
889 Land Information System and ParFlow Environment, *J Adv Model Earth Sy*, 17, e2024MS004415,  
890 <https://doi.org/10.1029/2024MS004415>, 2025.

891 Martin, M. H.: Conditions Affecting the Distribution of *Mercurialis Perennis* L. in Certain Cambridgeshire  
892 Woodlands, *Journal of Ecology*, 56, 777-793, 10.2307/2258106, 1968.

893 Maxwell, R. M.: A terrain-following grid transform and preconditioner for parallel, large-scale,  
894 integrated hydrologic modeling, *Adv Water Resour*, 53, 109-117,  
895 <https://doi.org/10.1016/j.advwatres.2012.10.001>, 2013.

896 Maxwell, R. M. and Condon, L. E.: Connections between groundwater flow and transpiration  
897 partitioning, *Science*, 353, 377-380, 2016.

898 Maxwell, R. M. and Miller, N. L.: Development of a coupled land surface and groundwater model, *J*  
899 *Hydrometeorol*, 6, 233-247, 2005.

900 Maxwell, R. M., Chow, F. K., and Kollet, S. J.: The groundwater–land–surface–atmosphere connection:  
901 Soil moisture effects on the atmospheric boundary layer in fully-coupled simulations, *Adv Water Resour*,  
902 30, 2447-2466, <https://doi.org/10.1016/j.advwatres.2007.05.018>, 2007.

903 Maxwell, R. M., Condon, L. E., and Kollet, S. J.: A high-resolution simulation of groundwater and surface  
904 water over most of the continental US with the integrated hydrologic model ParFlow v3, *Geosci Model*  
905 *Dev*, 8, 923-937, 10.5194/gmd-8-923-2015, 2015.

906 Maxwell, R. M., Lundquist, J. K., Mirocha, J. D., Smith, S. G., Woodward, C. S., and Tompson, A. F. B.:  
907 Development of a Coupled Groundwater-Atmosphere Model, *Mon Weather Rev*, 139, 96-116,  
908 10.1175/2010mwr3392.1, 2011.

909 Maxwell, R. M., Putti, M., Meyerhoffer, S., Delfs, J.-O., Ferguson, I. M., Ivanov, V., Kim, J., Kolditz, O., Kollet,  
910 S. J., Kumar, M., Lopez, S., Niu, J., Paniconi, C., Park, Y.-J., Phanikumar, M. S., Shen, C., Sudicky, E. A.,  
911 and Sulis, M.: Surface-subsurface model intercomparison: A first set of benchmark results to diagnose  
912 integrated hydrology and feedbacks, *Water Resour Res*, 50, 1531-1549,  
913 <https://doi.org/10.1002/2013WR013725>, 2014.

914 Miguez-Macho, G. and Fan, Y.: A global humidity index with lateral hydrologic flows, *Nature*, 644, 413-  
915 419, 10.1038/s41586-025-09359-3, 2025.

916 Mikkelsen, K. M., Maxwell, R. M., Ferguson, I., Stednick, J. D., McCray, J. E., and Sharp, J. O.: Mountain  
917 pine beetle infestation impacts: modeling water and energy budgets at the hill-slope scale, *Ecohydrology*, 6, 64-72, <https://doi.org/10.1002/eco.278>, 2013.

919 Muñoz-Sabater, J., Dutra, E., Agustí-Panareda, A., Albergel, C., Arduini, G., Balsamo, G., Boussetta, S.,  
920 Choulga, M., Harrigan, S., Hersbach, H., Martens, B., Miralles, D. G., Piles, M., Rodríguez-Fernández, N.  
921 J., Zsoter, E., Buontempo, C., and Thépaut, J. N.: ERA5-Land: a state-of-the-art global reanalysis dataset  
922 for land applications, *Earth Syst. Sci. Data*, 13, 4349-4383, 10.5194/essd-13-4349-2021, 2021.

923 Niu, G.-Y., Paniconi, C., Troch, P. A., Scott, R. L., Durcik, M., Zeng, X., Huxman, T., and Goodrich, D. C.:  
924 An integrated modelling framework of catchment-scale ecohydrological processes: 1. Model  
925 description and tests over an energy-limited watershed, *Ecohydrology*, 7, 427-439,  
926 <https://doi.org/10.1002/eco.1362>, 2014.

927 Niu, G.-Y., Yang, Z.-L., Mitchell, K. E., Chen, F., Ek, M. B., Barlage, M., Kumar, A., Manning, K., Niyogi, D.,  
928 Rosero, E., Tewari, M., and Xia, Y.: The community Noah land surface model with multiparameterization  
929 options (Noah-MP): 1. Model description and evaluation with local-scale measurements, *Journal of*  
930 *Geophysical Research: Atmospheres*, 116, <https://doi.org/10.1029/2010JD015139>, 2011.

931 O'Neill, M. M. F., Tijerina, D. T., Condon, L. E., and Maxwell, R. M.: Assessment of the ParFlow-CLM  
932 CONUS 1.0 integrated hydrologic model: evaluation of hyper-resolution water balance components  
933 across the contiguous United States, *Geosci. Model Dev.*, 14, 7223-7254, 10.5194/gmd-14-7223-2021,  
934 2021.

935 Oleson, K. W., Niu, G. Y., Yang, Z. L., Lawrence, D. M., Thornton, P. E., Lawrence, P. J., Stöckli, R.,  
936 Dickinson, R. E., Bonan, G. B., Levis, S., Dai, A., and Qian, T.: Improvements to the Community Land  
937 Model and their impact on the hydrological cycle, *Journal of Geophysical Research: Biogeosciences*,  
938 113, <https://doi.org/10.1029/2007JG000563>, 2008.

939 Osei-Kuffuor, D., Maxwell, R. M., and Woodward, C. S.: Improved numerical solvers for implicit coupling  
940 of subsurface and overland flow, *Adv Water Resour*, 74, 185-195,  
941 <https://doi.org/10.1016/j.advwatres.2014.09.006>, 2014.

942 Poll, S., Rigor, P., van Hulten, M., Patakchi Yousefi, K., Caviedes Voullieme, D., Goergen, K., and Kollet,  
943 S. J.: The new version of the Terrestrial Systems Modeling Platform (TSMP2) based on ICON, eCLM, and  
944 ParFlow, AGU Fall Meeting Abstracts, A32F-01,

945 Rahman, M., Sulis, M., and Kollet, S. J.: The subsurface-land surface-atmosphere connection under  
946 convective conditions, *Adv Water Resour*, 83, 240-249, 10.1016/j.advwatres.2015.06.003, 2015.

947 Raupach, M. R.: Drag and drag partition on rough surfaces, *Boundary-Layer Meteorology*, 60, 375-395,  
948 10.1007/BF00155203, 1992.

949 Raupach, M. R.: Simplified expressions for vegetation roughness length and zero-plane displacement  
950 as functions of canopy height and area index, *Boundary-Layer Meteorology*, 71, 211-216,  
951 10.1007/BF00709229, 1994.

952 Reinecke, R., Foglia, L., Mehl, S., Trautmann, T., Cáceres, D., and Döll, P.: Challenges in developing a  
953 global gradient-based groundwater model (G3M v1.0) for the integration into a global hydrological  
954 model, *Geosci. Model Dev.*, 12, 2401-2418, 10.5194/gmd-12-2401-2019, 2019.

955 Rihani, J. F., Chow, F. K., and Maxwell, R. M.: Isolating effects of terrain and soil moisture heterogeneity  
956 on the atmospheric boundary layer: Idealized simulations to diagnose land-atmosphere feedbacks, *J*  
957 *Adv Model Earth Sy*, 7, 915-937, <https://doi.org/10.1002/2014MS000371>, 2015.

958 Rihani, J. F., Maxwell, R. M., and Chow, F. K.: Coupling groundwater and land surface processes:  
959 Idealized simulations to identify effects of terrain and subsurface heterogeneity on land surface energy  
960 fluxes, *Water Resour Res*, 46, 2010.

961 Scanlon, B. R., Zhang, Z., Save, H., Sun, A. Y., Müller Schmied, H., van Beek, L. P. H., Wiese, D. N., Wada,  
962 Y., Long, D., Reedy, R. C., Longuevergne, L., Döll, P., and Bierkens, M. F. P.: Global models underestimate  
963 large decadal declining and rising water storage trends relative to GRACE satellite data, *Proceedings of*  
964 *the National Academy of Sciences*, 115, E1080-E1089, doi:10.1073/pnas.1704665115, 2018.

965 Schenk, H. J. and Jackson, R. B.: Mapping the global distribution of deep roots in relation to climate and  
966 soil characteristics, *Geoderma*, 126, 129-140, <https://doi.org/10.1016/j.geoderma.2004.11.018>, 2005.

967 Seuffert, G., Gross, P., Simmer, C., and Wood, E. F.: The Influence of Hydrologic Modeling on the  
968 Predicted Local Weather: Two-Way Coupling of a Mesoscale Weather Prediction Model and a Land  
969 Surface Hydrologic Model, *J Hydrometeorol*, 3, 505-523, [https://doi.org/10.1175/1525-7541\(2002\)003<0505:TIOHMO>2.0.CO;2](https://doi.org/10.1175/1525-7541(2002)003<0505:TIOHMO>2.0.CO;2), 2002.

970 Shangguan, W., Dai, Y., Duan, Q., Liu, B., and Yuan, H.: A global soil data set for earth system modeling,  
971 *J Adv Model Earth Sy*, 6, 249-263, 10.1002/2013ms000293, 2014.

972 Shen, C., Riley, W. J., Smithgall, K. R., Melack, J. M., and Fang, K.: The fan of influence of streams and  
973 channel feedbacks to simulated land surface water and carbon dynamics, *Water Resour Res*, 52, 880-  
974 902, <https://doi.org/10.1002/2015WR018086>, 2016.

976 Shrestha, P., Sulis, M., Masbou, M., Kollet, S., and Simmer, C.: A Scale-Consistent Terrestrial Systems  
977 Modeling Platform Based on COSMO, CLM, and ParFlow, *Mon Weather Rev*, 142, 3466-3483,  
978 <https://doi.org/10.1175/MWR-D-14-00029.1>, 2014.

979 Skamarock, W. C. and Klemp, J. B.: A time-split nonhydrostatic atmospheric model for weather research  
980 and forecasting applications, *Journal of Computational Physics*, 227, 3465-3485,  
981 <https://doi.org/10.1016/j.jcp.2007.01.037>, 2008.

982 Sperry, J. S. and Hacke, U. G.: Desert shrub water relations with respect to soil characteristics and plant  
983 functional type, *Funct Ecol*, 16, 367-378, <https://doi.org/10.1046/j.1365-2435.2002.00628.x>, 2002.

984 Sulis, M., Meyerhoff, S. B., Paniconi, C., Maxwell, R. M., Putti, M., and Kollet, S. J.: A comparison of two  
985 physics-based numerical models for simulating surface water-groundwater interactions, *Adv Water*  
986 *Resour*, 33, 456-467, <https://doi.org/10.1016/j.advwatres.2010.01.010>, 2010.

987 Sulis, M., Williams, J. L., Shrestha, P., Diederich, M., Simmer, C., Kollet, S. J., and Maxwell, R. M.:  
988 Coupling Groundwater, Vegetation, and Atmospheric Processes: A Comparison of Two Integrated  
989 Models, *J Hydrometeorol*, 18, 1489-1511, <https://doi.org/10.1175/JHM-D-16-0159.1>, 2017.

990 Sutanudjaja, E. H., van Beek, L. P. H., de Jong, S. M., van Geer, F. C., and Bierkens, M. F. P.: Calibrating  
991 a large-extent high-resolution coupled groundwater-land surface model using soil moisture and  
992 discharge data, *Water Resour Res*, 50, 687-705, <https://doi.org/10.1002/2013WR013807>, 2014.

993 Tai, X., Mackay, D. S., Sperry, J. S., Brooks, P., Anderegg, W. R. L., Flanagan, L. B., Rood, S. B., and  
994 Hopkinson, C.: Distributed Plant Hydraulic and Hydrological Modeling to Understand the Susceptibility  
995 of Riparian Woodland Trees to Drought-Induced Mortality, *Water Resour Res*, 54, 4901-4915,  
996 <https://doi.org/10.1029/2018WR022801>, 2018.

997 Tian, W., Li, X., Cheng, G. D., Wang, X. S., and Hu, B. X.: Coupling a groundwater model with a land  
998 surface model to improve water and energy cycle simulation, *Hydrol. Earth Syst. Sci.*, 16, 4707-4723,  
999 10.5194/hess-16-4707-2012, 2012.

1000 Tran, H., Leonarduzzi, E., De la Fuente, L., Hull, R. B., Bansal, V., Chennault, C., Gentine, P., Melchior, P.,  
1001 Condon, L. E., and Maxwell, R. M.: Development of a Deep Learning Emulator for a Distributed  
1002 Groundwater-Surface Water Model: ParFlow-ML, *Water*, 13, 3393, 2021.

1003 Valcke, S.: Highlights from a Workshop on the Latest Updates on Coupling Technologies and Coupled  
1004 Applications in Earth System Modeling, *B Am Meteorol Soc*, 103, E657-E664,  
1005 <https://doi.org/10.1175/BAMS-D-21-0045.1>, 2022.

1006 van den Hurk, B., Kim, H., Krinner, G., Seneviratne, S. I., Derksen, C., Oki, T., Douville, H., Colin, J.,  
1007 Ducharne, A., Cheruy, F., Viovy, N., Puma, M. J., Wada, Y., Li, W., Jia, B., Alessandri, A., Lawrence, D. M.,  
1008 Weedon, G. P., Ellis, R., Hagemann, S., Mao, J., Flanner, M. G., Zampieri, M., Matera, S., Law, R. M., and  
1009 Sheffield, J.: LS3MIP (v1.0) contribution to CMIP6: the Land Surface, Snow and Soil moisture Model  
1010 Intercomparison Project – aims, setup and expected outcome, *Geosci. Model Dev.*, 9, 2809-2832,  
1011 10.5194/gmd-9-2809-2016, 2016.

1012 Verkaik, J., Sutanudjaja, E. H., Oude Essink, G. H. P., Lin, H. X., and Bierkens, M. F. P.: GLOBGM v1.0: a  
1013 parallel implementation of a 30 arcsec PCR-GLOBWB-MODFLOW global-scale groundwater model,  
1014 *Geosci. Model Dev. Discuss.*, 2022, 1-27, 10.5194/gmd-2022-226, 2022.

1015 Vogelbacher, A., Afshar, M. H., Aminzadeh, M., Madani, K., AghaKouchak, A., and Shokri, N.: A global  
1016 analysis of the influence of shallow and deep groundwater tables on relationships between  
1017 environmental parameters and heatwaves inferred from machine learning models, *Environmental*  
1018 *Research*, 123354, <https://doi.org/10.1016/j.envres.2025.123354>, 2025.

1019 Wagg, J. B.: Origin and development of White Spruce root-forms, 1967.

1020 West, B. D., Maxwell, R. M., and Condon, L. E.: A scalable and modular reservoir implementation for  
1021 large-scale integrated hydrologic simulations, *Hydrol. Earth Syst. Sci.*, 29, 245-259, 10.5194/hess-29-  
1022 245-2025, 2025.

1023 Williams, J. L. and Maxwell, R. M.: Propagating Subsurface Uncertainty to the Atmosphere Using Fully  
1024 Coupled Stochastic Simulations, *J Hydrometeorol*, 12, 690-701,  
1025 <https://doi.org/10.1175/2011JHM1363.1>, 2011.

1026 Xu, G.-Q. and Li, Y.: Rooting depth and leaf hydraulic conductance in the xeric tree *Haloxyylon*  
1027 *ammodendron* growing at sites of contrasting soil texture, *Functional Plant Biology*, 35, 1234-1242,  
1028 10.1071/fp08175, 2008.

1029 Xue, M., Droegemeier, K. K., and Wong, V.: The Advanced Regional Prediction System (ARPS) – A multi-  
1030 scale nonhydrostatic atmospheric simulation and prediction model. Part I: Model dynamics and  
1031 verification, *Meteorol Atmos Phys*, 75, 161-193, 10.1007/s007030070003, 2000.

1032 Xue, M., Droegemeier, K. K., Wong, V., Shapiro, A., Brewster, K., Carr, F., Weber, D., Liu, Y., and Wang,  
1033 D.: The Advanced Regional Prediction System (ARPS) – A multi-scale nonhydrostatic atmospheric  
1034 simulation and prediction tool. Part II: Model physics and applications, *Meteorol Atmos Phys*, 76, 143-  
1035 165, 10.1007/s007030170027, 2001.

1036 Yang, C., Maxwell, R., McDonnell, J., Yang, X., and Tijerina-Kreuzer, D.: The Role of Topography in  
1037 Controlling Evapotranspiration Age, *Journal of Geophysical Research: Atmospheres*, 128,  
1038 e2023JD039228, <https://doi.org/10.1029/2023JD039228>, 2023.

1039 Yang, C., Jia, Z., Xu, W., Wei, Z., Zhang, X., Zou, Y., McDonnell, J., Condon, L., Dai, Y., and Maxwell, R.:  
1040 CONCN: a high-resolution, integrated surface water–groundwater ParFlow modeling platform of  
1041 continental China, *Hydrol. Earth Syst. Sci.*, 29, 2201-2218, 10.5194/hess-29-2201-2025, 2025.

1042 Yang, C., Li, H.-Y., Fang, Y., Cui, C., Wang, T., Zheng, C., Leung, L. R., Maxwell, R. M., Zhang, Y.-K., and  
1043 Yang, X.: Effects of Groundwater Pumping on Ground Surface Temperature: A Regional Modeling Study  
1044 in the North China Plain, *Journal of Geophysical Research: Atmospheres*, 125, e2019JD031764,  
1045 10.1029/2019jd031764, 2020.

1046 Yeh, P. J. F. and Eltahir, E. A. B.: Representation of Water Table Dynamics in a Land Surface Scheme.  
1047 Part I: Model Development, *J Climate*, 18, 1861-1880, <https://doi.org/10.1175/JCLI3330.1>, 2005.

1048 York, J. P., Person, M., Gutowski, W. J., and Winter, T. C.: Putting aquifers into atmospheric simulation  
1049 models: an example from the Mill Creek Watershed, northeastern Kansas, *Adv Water Resour*, 25, 221-  
1050 238, [https://doi.org/10.1016/S0309-1708\(01\)00021-5](https://doi.org/10.1016/S0309-1708(01)00021-5), 2002.

1051 Yuan, H. and Dai, Y.: Description of the Common Land Model (CoLM 2024), Sun Yat-sen University Press,  
1052 Guangzhou, China, 2025.

1053 Yuan, H., Dickinson, R. E., Dai, Y., Shaikh, M. J., Zhou, L., Shangguan, W., and Ji, D.: A 3D Canopy Radiative  
1054 Transfer Model for Global Climate Modeling: Description, Validation, and Application, *J Climate*, 27,  
1055 1168-1192, <https://doi.org/10.1175/JCLI-D-13-00155.1>, 2014.

1056 Yuan, H., Dai, Y., Dickinson, R. E., Pinty, B., Shangguan, W., Zhang, S., Wang, L., and Zhu, S.:  
1057 Reexamination and further development of two-stream canopy radiative transfer models for global  
1058 land modeling, *J Adv Model Earth Sy*, 9, 113-129, <https://doi.org/10.1002/2016MS000773>, 2017.

1059 Zeng, Y. J., Xie, Z. H., Liu, S., Xie, J. B., Jia, B. H., Qin, P. H., and Gao, J. Q.: Global Land Surface Modeling  
1060 Including Lateral Groundwater Flow, *J Adv Model Earth Sy*, 10, 1882-1900, 10.1029/2018ms001304,  
1061 2018.

1062